International Journal of Multiphase Flow 35 (2009) 1–7

Contents lists available at ScienceDirect

International Journal of Multiphase Flow

journal homepage: www.elsevier.com/locate/ijmulflow

Maximum spreading of electrically charged droplets impacting on dielectric substrates

Sung Uk Ryu, Sang Yong Lee *

Department of Mechanical Engineering, KAIST, Science Town, Daejeon 305-701, Republic of Korea

ARTICLE INFO

Article history:
Received 11 February 2008
Received in revised form 21 July 2008
Accepted 15 September 2008
Available online 27 September 2008

Keywords:
Electrically charged droplet
Single-droplet impact
Maximum spreading ratio
Modified interfacial tensions
Dielectric substrates

ABSTRACT

In this work, the electric charging effect on the spreading of droplet impacting on dielectric substrates has been investigated. The charged water droplets were directed on the paraffin wax and the Teflon-coated plates. The impinging behavior was visualized and recorded using a CCD camera to identify the maximum extent of the flattened droplets. Droplet diameter and velocity approaching the wall were measured as well. The diameter of the electrically charged droplet at the maximum spread turned out to be larger compared to that of neutral droplet (at the maximum spread), and the difference becomes larger with increasing of the electric charge ratio (defined as the ratio of the actual electric charge to the Rayleigh limit). This phenomenon is considered to be due to reduction of effective interfacial tensions between the liquid and the gas and between the liquid and the solid by electric charging. Finally, an improved model was proposed to predict the maximum spreading ratio for electrically charged droplets by introducing correlations on the liquid–gas and the liquid–solid interfacial tensions.

1. Introduction

The impingement phenomenon of electrically charged droplets is widely seen in many applications such as electrostatic spraying, surface coating (wall deposition of droplets), agricultural sprays, and ink-jet printing. The electrostatic spraying and the ink-jet printing, in particular, are considered highly competitive alternative technologies in manufacturing of thin films for plasma display panels and implants. Thus, there is a need for further studies on the impinging behavior of the charged droplets, particularly with respect to post-impingement regimes and maximum spreading ratio.

The maximum spreading ratio (β_{max}) of droplets, expressed as the ratio of the maximum extent of droplet (D_{max}) to the droplet diameter (d), is a primary parameter for predicting post-impingement regimes and the spreading area of the droplets:

$$\beta_{max} = \frac{D_{max}}{d}. \quad (1)$$

A number of works have focused on modeling the maximum extent of a spread, particularly by Chandra and Avedisian (1991), Pasandideh-Fard et al. (1996), Mao et al. (1997), Park et al. (2003) and Ryu and Lee (in press). They have proposed theoretical models based on the application of mass and energy conservation in relation to the pre-impact state and the maximum spread state. They also compared the models with the measured values to show how well the models represent the maximum spreading ratio. The accuracy of those models depends on the correlations on the surface energy at the maximum spread and the dissipated energy during the spreading process. Several correlations on the dissipated energy have been proposed by Pasandideh-Fard et al. (1996), Mao et al. (1997) and Park et al. (2003), all based on the concept of Chandra and Avedisian (1991). The underlying assumption of such proposals is that the shape of the droplets at a maximum spread, which is a key feature in estimating the surface energy, must resemble either a cylindrical disk or a spherical cap. Ryu and Lee (in press) subsequently showed from the visualized images that the actual shape is similar to a half-torus and proposed an improved maximum spread model based on that configuration.

All the above studies on the maximum spread of droplets were performed for electrically neutral cases and, thus, may not be suitable for predicting the impinging behavior of charged droplets. When a droplet is electrically charged, the liquid–gas and liquid–solid interfacial tensions are expected to be changed, and accordingly, the wettability of the wall surface is varied. The surface wettability represented by the static contact angle is known to be an important factor determining the maximum spread (Mao et al., 1997; Ryu and Lee, in press). We therefore expect the spreading behavior of electrically charged droplets to differ from that of neutral droplets. Because of the application of charged droplets in electrowetting and electrostatic spraying, many researchers have studied how electric fields and charged droplets affect surface wettability (Bateni et al., 2005, 2006; Digilov, 2000; Kang et al., 2003; Lee et al., 2002; Vallet et al., 1996). Many studies related to electrowetting phenomena have shown that the effect of electric charging on liquid wettability can be described with the Lippmann–Young

* Corresponding author. Tel.: +82 42 350 3026; fax: +82 42 350 8207.
E-mail address: sangyonglee@kaist.ac.kr (S.Y. Lee).

0301-9322/$ - see front matter © 2008 Elsevier Ltd. All rights reserved.
doi:10.1016/j.ijmultiphaseflow.2008.09.003

equation. This equation is based on the assumption that the liquid–gas interfacial tension and the solid–gas interfacial tension are unaffected by electric charging, and that the variation of wettability is a consequence of the change in the liquid–solid interfacial tension only. Recently, Bateni et al. (2005, 2006) proposed that changes in the liquid–solid interfacial tension and the liquid–gas interfacial tension should be considered simultaneously to obtain more accurate results. The researches on the wall impingement of charged droplets may be categorized to several cases; whether the electric field is imposed or not and the substrate is electrically conductive or not. Existence of the electric field changes the trajectories and velocities of the droplets approaching the wall. When the charged droplets are impinging on the conductive substrate, the droplets are neutralized by electric discharge to the ground. However, when the dielectric substrate is used, the droplets retain the electrons that make the impinging behavior (motion of droplets) different from that of the neutralized droplets.

In this study, for better prediction of the maximum spread of the charged droplets, behavior the droplets impacting against dielectric substrates was carefully visualized and the analytical model was improved to take account of the charging effect. Such an improvement could be realized by modification of the models on liquid–gas and liquid–solid interfacial forces of the liquid droplet, which is affected by the electric charge quantity and shape of the droplets. Because the substrate was dielectric, the electric discharge from droplets to the ground could be neglected and the droplets remain charged throughout the spreading process.

2. Experimental setup and method

In order to observe the spreading behavior of an impinging droplet onto the solid wall, a simple experimental setup was constructed as shown in Fig. 1.

Water was supplied by a syringe pump through a flat-tipped stainless-steel needle, and was electrically charged by imposing a high voltage ranging from 2.6 to 3.7 kV between the needle and a ring electrode at the exit using a power supply. The ring electrode is located at 10 mm downstream from the needle tip.

Droplet size was controlled by adjusting the liquid flow rate and imposed voltage as well as by changing the needle size. Four different needles were used: 140 (gage 30), 241 (gage 26), 292 (gage 24), 838 (gage 18) μm in internal diameter.

A vertical glass tube (26 mm ID, ranging from 50 to 300 mm in length corresponding to the distance between the needle and the substrate to control the velocity of the falling droplets approaching the substrate) was vertically placed 15 mm below the needle tip to let the droplet pass through without being disturbed by the ambient air. At the bottom exit of the glass tube, an infrared laser (LTC100-B, Thorlabs) and an optical sensor (PDA50B-EC, Thorlabs) were aligned in transverse direction. A 5 V pulse was generated by the optical sensor when the droplet crossed the laser beam. A stroboscope and a CCD camera (Sensicam, PCO) activated by the pulse with a time delay (by a digital delay generator (DG-535, SRS)) were used for visualization of the droplet behavior. The time delay was adjusted to capture images at different instances after the initial impact and the time resolution was about 5 ps. A series of photographs showing the impact process were acquired by using the above-mentioned visualization technique. Fig. 2 shows three different droplet images at the same delay time to confirm the accuracy of the visualization method. As evidenced in the figure, the shapes of the droplets appear almost identical and the experimental setup and the method are considered appropriate for identifying the impact sequence of a droplet.

The CCD camera was positioned on a rotating platform (GOH-60A50, Sigma KOKI) to observe the deformed droplet more clearly.

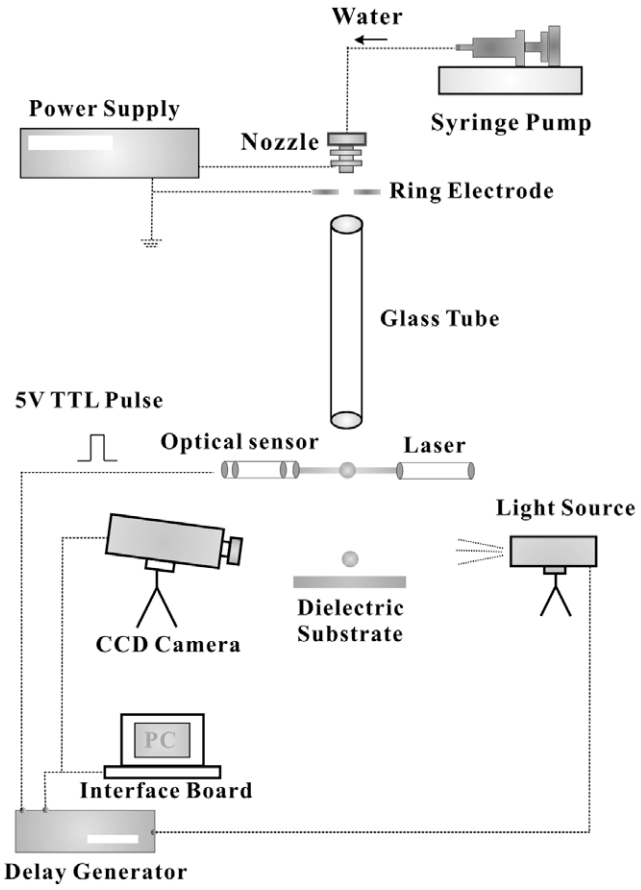

Fig. 1. Experimental setup.

The size of the droplets before the impingement was measured directly from the photographs. Since the droplets are not in perfectly spherical shape, the equivalent diameter has been obtained by measuring the diameter in horizontal direction (d_h) and the length in vertical direction (d_v) assuming the droplet has an axisymmetric ellipsoidal shape

$$d = \left(d_h^2 d_v\right)^{1/3}. \quad (2)$$

Size of the droplets tested in the present experiment ranged from 1.35 to 3.15 mm.

Likewise, the velocity of the falling droplets was estimated from the distances between the droplet images and the time interval(s) of the double (or multiple) exposures, and ranged from 0.6 to 2.1 m/s. The estimated uncertainties of the droplets diameter and velocity measurements were ±0.5% and ±1%, respectively. The uncertainty analysis has been performed according to the method proposed by Kline (1985).

Distilled water in an ambient temperature (T = 20 °C) was used as the test fluid. A paraffin wax plate and a Teflon-coated plate at the ambient temperature were used as the substrates. To eliminate the remains of the previous impinging droplets from the substrate, the surface was dried by using an air blower. Thereby, the surface could be kept in a completely dry condition and the dry-wall impingement behavior of a single droplet could be examined.

The electric charges remaining on the substrate surface may cause an unexpected effect on the spreading behavior of charged droplet. Thus, in the present study, to exclude the effect of remained charges, they were removed by rolling an earthed metal cylinder over the surface of the substrates prior to each droplet impact.

Fig. 2. Three different droplet images at the same delay time (delay time: 18.5 ms).

As reported by Mao et al. (1997), the static contact angle of a droplet on a substrate is an important parameter determining the droplet impinging behavior. Also, the electric charge of impinging droplet was expected to be another parameter. Therefore, prior to the main test, the static contact angle, surface roughness amplitude and the amount of the electric charge were measured using a contact-angle tester (G10, KRÜSS GmbH), roughness tester (SJ-400, Mitutoyo) and an electrometer (6514, Keithley). Since the measurement of the charged quantity of an individual droplet induces unacceptable error, the specific charge of droplet was obtained by dividing the charge collected in the Faraday cage by the number of droplets. In this case, the droplet size was confirmed uniform at each experimental condition, and the amount of electric charge carried by each droplet was expected to be the same as well.

The static contact angles of electrically neutral water droplets on the paraffin wax plate and on the Teflon-coated plate were measured to be 118° and 110°, respectively, and the mean surface roughness amplitudes of the paraffin wax plate and the Teflon-coated plate were 0.25 and 0.31 μm, respectively.

3. Results

3.1. Phenomenological observation

The spreading processes of droplets impacting on the dielectric substrate were examined for droplet Weber numbers $\left(We = \rho_L V_{b,n}^2 d/\gamma_{LG}\right)$ ranging from 12 to 89 and droplet Reynolds numbers ($Re = \rho_L V_{b,n} d/\mu_L$) from 1100 to 4470. Here, ρ_L is the liquid density, $V_{b,n}$ the droplet normal velocity prior to the wall impact, γ_{LG} the liquid–gas interfacial (surface) tension and μ_L the liquid viscosity.

Fig. 3(a) and (b) shows the sequential motion of electrically neutral and charged water droplets on the paraffin wax substrate at room temperature ($T = 20$ °C), respectively. The impact processes of both the neutral droplet and the electrically charged droplet consist of three distinct stages: the spreading stage, the maximum spread stage, and the recoil stage. Furthermore, the visualized images confirm that the droplet shape at the maximum spread stage resembles a half-torus regardless of electric charging.

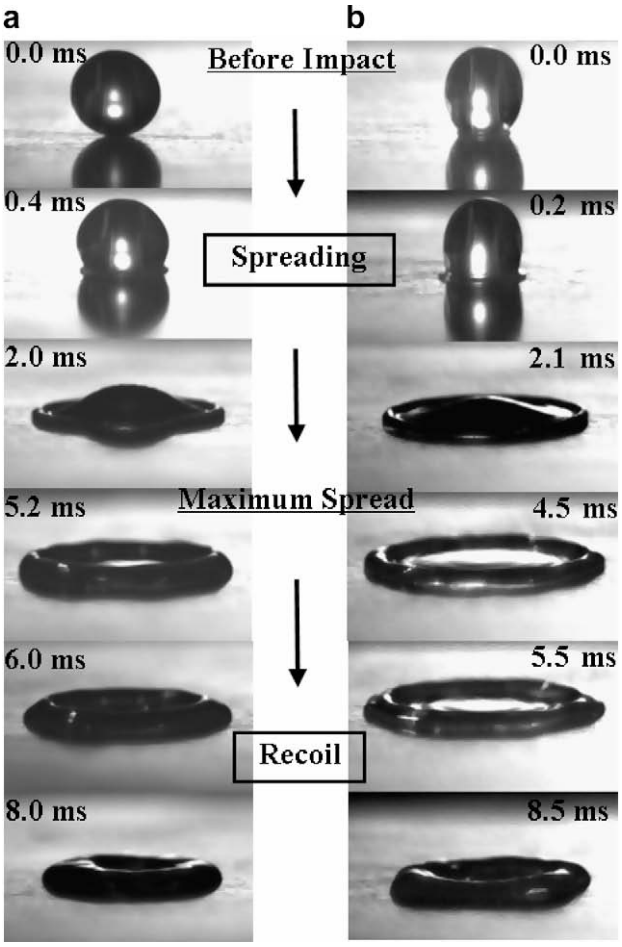

Fig. 3. Impact of a water droplet on paraffin wax. (a) Electrically neutral droplet ($d = 3.05$ mm, $V_{b,n} = 1.13$ m/s). (b) Electrically charged droplet ($d = 2.99$ mm, $V_{b,n} = 1.25$ m/s).

3.2. Maximum spreading ratio

3.2.1. Experimental results

In Fig. 4, the measured values of the maximum spreading ratio (β_{max}, Eq. (1)) were compared with the values from the correlation of Ryu and Lee (in press), originally developed for electrically neutral droplets impinging on the wall as follows:

$$\left\{\alpha(1-\alpha)\left(\frac{\pi}{2}-\cos\theta\right)+0.43\frac{We^{0.67}}{Re^{0.30}}\right\}(\beta_{max})^2-\left(\frac{We}{12}+1\right)=0, \tag{3}$$

$$(\beta_{max})^3=\frac{4}{3\pi}\frac{1}{\alpha^2(1-\alpha)} \quad (\text{for } 0<\alpha<2/3). \tag{4}$$

Here, θ is the static contact angle, We the droplet Weber number and Re the droplet Reynolds number. As illustrated in Fig. 5, parameter α in Eqs. (3) and (4) is the ratio of the rim thickness (D_{rim}) to the diameter of the liquid torus (D_{max}). Eqs. (3) and (4) were derived for the ranges of the Weber numbers of 10–120 and Reynolds numbers of 1500–4700.

As shown in Fig. 4, the measured values of the neutral droplet were confirmed to be in agreement with the predicted values. On the other hand, for the charged droplets, the measured values appeared larger than the predicted ones and the difference appeared prominent as the charge ratio (q/q_{Ray}) was increased. Here, the charge ratio is defined as the ratio of the actual charge (q) to the Rayleigh charge limit (q_{Ray}). The Rayleigh limit is, as expressed in Eq. (5), the maximum electric charge that a single droplet can carry theoretically (Bailey, 1988):

$$q_{Ray}=8\pi(\varepsilon_0\gamma_{LG}r^3)^{1/2} \tag{5}$$

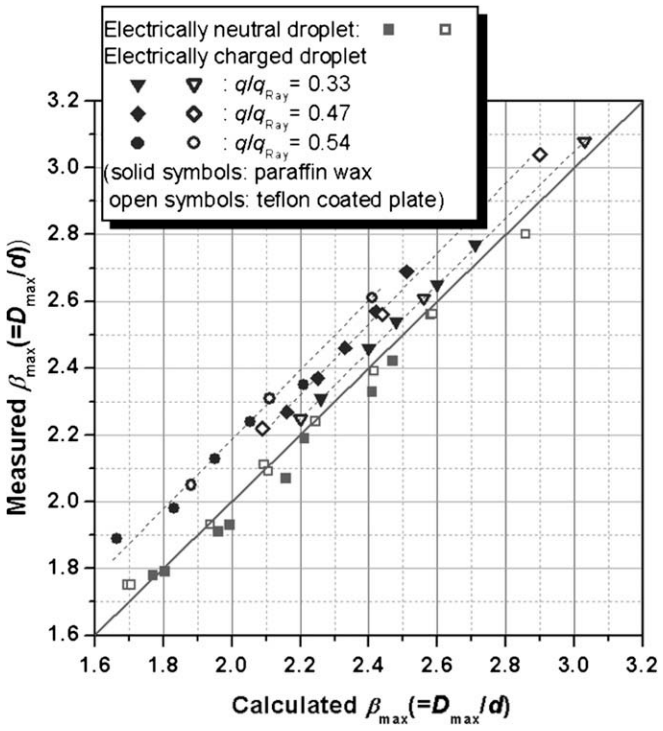

Fig. 4. Comparison of the maximum spreading ratio between the model by Ryu and Lee (in press) and the present experimental data.

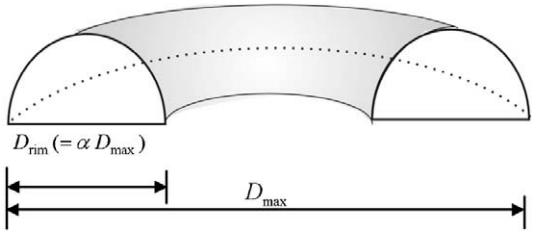

Fig. 5. Cross section of the liquid film at the maximum spread state.

Here, ε_0 is permittivity of the free space (=8.854 × 10^{-12} C^2/N m^2) and r is the droplet radius.

The present experimental result shows that, firstly, the maximum spreading ratio of the electrically charged droplets is larger than that of the neutral droplets when the impacting conditions remain unchanged and, secondly, the charge ratio is the one of the primary parameters affecting the spreading behavior of the charged droplets. This implies that Eq. (3) has to be modified to take into account the electric charge effect.

3.2.2. Modified interfacial tension

In Eq. (3), the important parameters for determining the droplet spreading behavior are *We*, Re and θ. Variable α in Eq. (3) is an intermediate dependent parameter that can be obtained by using Eq. (4). Of the three major parameters, *We* and θ depend on the gas-liquid and solid–liquid interfacial tensions, which is affected by the amount of electric charging.

For a spherical droplet, the surface energy (E_S) by the liquid–gas interfacial (surface) tension (γ_{LG}) is written as

$$E_S = 4\pi r^2 \gamma_{LG} \tag{6}$$

and the electric potential energy (E_e) by the surface charge is obtained to be as follows:

$$E_e = \frac{q^2}{8\pi\varepsilon_0 r}. \tag{7}$$

Hence, for an electrically neutral droplet, there exists only an inward radial force (F), corresponding to the surface tension, to form a spherical interface:

$$F = \frac{\partial E_S}{\partial r} = 8\pi r \gamma_{LG}. \tag{8}$$

Note that the force shown in Eq. (8) is the same as the pressure difference between the inside and outside of the droplet ($2\gamma_{LG}/r$) multiplied by the surface area ($4\pi r^2$).

On the other hand, for an electrically charged spherical droplet, there is another force acts in the opposite (outward) direction originated from the repulsive forces between the charges. Thus, from Eqs. (5)–(7), the net radial force ($F^{(c)}$) exerted on the surface in the inward direction (for a charged droplet) appears as:

$$F^{(c)} = \frac{\partial(E_S + E_e)}{\partial r} = 8\pi r \gamma_{LG}\left(1 - \left(\frac{q}{q_{Ray}}\right)^2\right). \tag{9}$$

Hence, the net force for a charged spherical droplet (Eq. (9)) can be written in the form of Eq. (8) by introducing a modified liquid–gas interfacial tension $\left(\gamma_{LG}^{(c)}\right)$, expressed as follows:

$$\gamma_{LG}^{(c)} = \gamma_{LG}\left\{1 - \left(\frac{q}{q_{Ray}}\right)^2\right\} \quad (\text{for } q < q_{Ray}). \tag{10}$$

According to Eq. (10), the effective liquid–gas interfacial tension becomes zero when the droplet charge reaches the Rayleigh limit, and the droplet can be disintegrated by itself without any external force exerted. The results similar to Eqs. (9) and (10) have been reported in the classical work by Rayleigh (1945).

Eq. (10) can be further modified for arbitrary-shaped droplets by considering the surface area change. As illustrated in Fig. 6, the mean surface-charge density, defined as the droplet charge per unit surface area, decreases by distortion of the droplet shape due to the increase of the surface area. Therefore, more electric charges (than the Rayleigh limit for spherical droplets) can be accommodated to the distorted droplets due to the increase of the surface area. Thus, to be applicable to droplets in arbitrary shape, Eq. (10) was modified by replacing the Rayleigh charge limit, q_{Ray}, with the maximum charge limit of a droplet in arbitrary shape, $(q_{max})_{arb}$, that is going to be discussed right after.

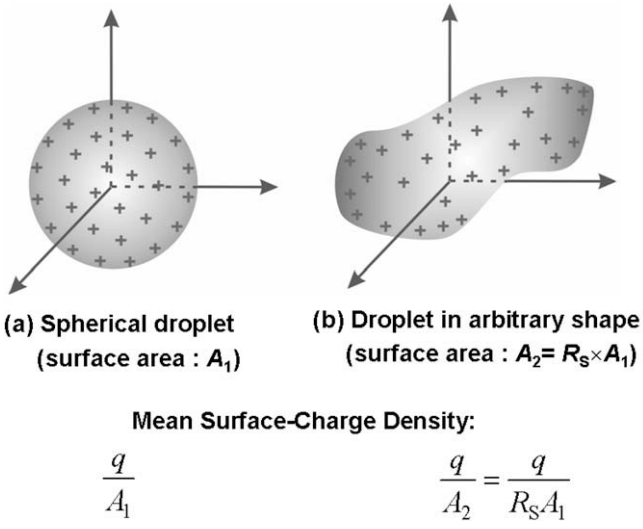

Fig. 6. Mean surface-charge density of droplets with different shapes.

Assuming that $(q_{max})_{arb}$ is directly proportional to the mean surface-charge density, it can be expressed in terms of the Rayleigh limit (q_{Ray}) and the surface area ratio (R_S):

$$(q_{max})_{arb} = R_S q_{Ray}. \tag{11}$$

Here, R_S implies the surface area ratio between the arbitrary-shaped droplet and the spherical droplet having the same volume; that is, R_S becomes the unity for a spherical droplet. Then an extended form of liquid–gas interfacial tension can be obtained for charged droplets in arbitrary shape as follows:

$$\gamma^{(c)}_{LG,arb} = \gamma_{LG}\left\{1 - \left(\frac{q}{q_{Ray}}\right)^2\left(\frac{1}{R_S^2}\right)\right\} \quad (\text{for } q < q_{Ray}). \tag{12}$$

According to Bateni et al. (2005, 2006), the change in both the liquid–solid interfacial tension (γ_{SL}) and liquid–gas interfacial tension (γ_{LG}) should be considered in analyzing the effect of electric charging on the surface wettability. For a droplet on a solid wall, γ_{SL} can be expressed as a function of the liquid–gas and solid–gas interfacial tensions (γ_{LG} and γ_{SG}) and the work of adhesion per unit area (w_{SL}) (Carey, 1992):

$$\gamma_{SL} = \gamma_{LG} + \gamma_{SG} - w_{SL}. \tag{13}$$

A number of works have been reported on the model for predicting w_{SL} (Fowkes, 1963; Girifalco and Good, 1957, 1958, 1960; Li and Neumann, 1990, 1992). Here, based on the model of Li and Neumann (1990, 1992), Eq. (13) is rearranged as

$$\gamma_{SL} = \gamma_{LG} + \gamma_{SG} - 2\sqrt{\gamma_{LG}\gamma_{SG}}\,e^{-j(\gamma_{LG}-\gamma_{SG})^2}, \tag{14}$$

where $j = 1.247 \times 10^2$ N/m^{-2}. By inserting Eq. (14) to the Young's equation (also see Fig. 7)

$$\cos\theta = \frac{\gamma_{SG} - \gamma_{SL}}{\gamma_{LG}}, \tag{15}$$

the contact angle can be rewritten only in terms of γ_{LG} and γ_{SG} as:

$$\cos\theta = -1 + 2\sqrt{\frac{\gamma_{SG}}{\gamma_{LG}}}\,e^{-j(\gamma_{LG}-\gamma_{SG})^2}. \tag{16}$$

Thus, from Eqs. (14) and (16), the values of γ_{SG} and γ_{SL} can be determined once the values of γ_{LG} and the contact angle (θ) are given. Here, γ_{SG} is known to be unaffected by the electric field or the droplet charging (Bateni et al., 2005, 2006; Digilov, 2000; Kang et al., 2003; Lee et al., 2002; Vallet et al., 1996). Therefore, γ_{SG} is assumed to remain the same irrespective of electric charging, and only the change of γ_{SL} has to be considered by electric charging. Hence, for a charged droplet in arbitrary shape, $\gamma^{(c)}_{SL,arb}$ can be obtained by using Eq. (14) along with the information on $\gamma^{(c)}_{LG,arb}$ (Eq. (12)) to predict the maximum spread as will be explained in the following section. In other words

$$\gamma^{(c)}_{SL,arb} = \gamma^{(c)}_{LG,arb} + \gamma_{SG} - 2\sqrt{\gamma^{(c)}_{LG,arb}\gamma_{SG}}\,e^{-j\left(\gamma^{(c)}_{LG,arb}-\gamma_{SG}\right)^2}. \tag{17}$$

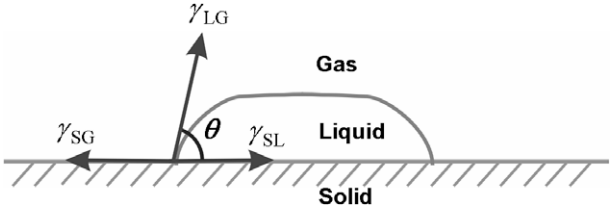

Fig. 7. Relationship between the interfacial tensions.

3.2.3. Modified maximum spread model for charged droplets

To obtain the maximum spreading ratio of electrically charged droplets, the concept of the energy conservation was adopted for the process of droplet impact as shown in Fig. 8 and the corresponding equation can be written as follows:

$$E_{K,1} + E_{S,1} = E_{S,2} + W_{diss}. \tag{18}$$

The left-hand side of Eq. (18) is the sum of the kinetic energy ($E_{K,1}$) and the surface energy ($E_{S,1}$) of the droplets before impact, respectively; this sum should be the same with the sum of the surface energy at the maximum spread ($E_{S,2}$) and the dissipated energy (W_{diss}) during the spread process as shown in the right-hand side terms, respectively. Here

$$E_{K,1} = \frac{1}{2}\left(\frac{1}{6}\rho_L \pi d^3\right)V_{b,n}^2, \tag{19}$$

$$E_{S,1} = \pi d^2 \gamma^{(c)}_{LG}, \tag{20}$$

and $\gamma^{(c)}_{LG}$ (for a charged spherical droplet) was already given in Eq. (10).

The term $E_{S,2}$ is equal to the sum of the surface energy at the liquid–gas interface $(E_{S,2})_{LG}$ and the surface energy difference between the liquid–solid interface $(E_{S,2})_{SL}$ and the solid–gas interface $(E_{S,2})_{SG}$ caused by change of the interfacial contact. That is

$$E_{S,2} = (E_{S,2})_{LG} + \{(E_{S,2})_{SL} - (E_{S,2})_{SG}\} \tag{21}$$

with

$$(E_{S,2})_{LG} = \frac{\pi^2}{2}\alpha(1-\alpha)D_{max}^2\left(\gamma^{(c)}_{LG,arb}\right)_{R_{S,max}}, \tag{22}$$

$$(E_{S,2})_{SL} - (E_{S,2})_{SG} = \pi\alpha(1-\alpha)D_{max}^2\left\{\left(\gamma^{(c)}_{SL,arb}\right)_{R_{S,max}} - \gamma_{SG}\right\}. \tag{23}$$

Here, based on the configuration of a half-torus, the surface–area ratio at the maximum spread ($R_{S,max}$) is given as follows:

$$R_{S,max} = \frac{(1+\frac{\pi}{2})\alpha(1-\alpha)\pi D_{max}^2}{\pi d^2} = \alpha(1-\alpha)\left(1+\frac{\pi}{2}\right)\beta_{max}^2. \tag{24}$$

For the dissipation energy term (W_{diss}) in Eq. (18), the following equation from the basic model of Mao et al. (1997) and the experimental data of Ryu and Lee (in press), is adopted along with γ_{LG} replaced by $\gamma^{(c)}_{LG}$:

$$\frac{W_{diss}}{\pi d^2 \gamma^{(c)}_{LG}} = 0.43\frac{We^{(c)^{0.67}}}{Re^{0.30}}(\beta_{max})^2. \tag{25}$$

Here

$$We^{(c)} = \frac{\rho_L V_{b,n}^2 d}{\gamma^{(c)}_{LG}}. \tag{26}$$

Then, by using Eqs. (19)–(21) and (25), we can rearrange the energy balance equation (Eq. (18)) as follows:

$$\alpha(1-\alpha)\beta_{max}^2\left\{\frac{\pi}{2}\left(1 - \frac{(q/q_{Ray})^2}{(R_{S,max})^2}\right) + \frac{\left(\gamma^{(c)}_{SL,arb}\right)_{R_{S,max}} - \gamma_{SG}}{\gamma_{LG}}\right\} + 0.43\frac{We^{0.67}}{Re^{0.30}}\beta_{max}^2\left(1 - (q/q_{Ray})^2\right)^{0.33} = \frac{We}{12} + 1 - (q/q_{Ray})^2. \tag{27}$$

This equation enables us to predict the maximum spreading ratio of both the electrically charged droplets and the neutral droplets. Eq. (27) reduces to Eq. (3) when q/q_{Ray} becomes zero. Eq. (4), which expresses the relation between parameters α and β_{max}, can be used

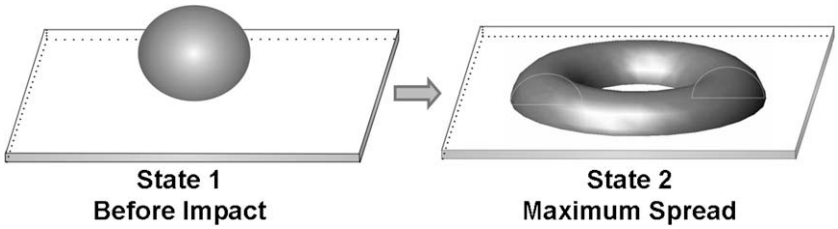

Fig. 8. Droplet before impact and at the maximum spread state.

also for the case of electrically charged droplets because this equation is based on the mass conservation of the droplets. The value of $\gamma^{(c)}_{SL,arb}$ can be determined from Eqs. (17) and (12), while γ_{SG} from Eq. (16), respectively.

To evaluate the accuracy of the improved model, the maximum spreading ratios predicted from the model were compared with the measured data as shown in Fig. 9; and the improved model represents most of the measured data within the range of ± 5%.

Even though the performance of the spread model has been improved for higher accuracy than the previous model, there is still some discrepancy between the measured and the predicted values. This is considered to be due to the assumptions made on the electric charge distribution along the droplet surface and the energy dissipation in the spreading process. Moreover, the half-torus assumption for the spread droplet shape does not consider a possibility of the presence of thin liquid layer in the center portion. In the present model, for simplicity, the surface charge distribution was assumed to be uniform regardless of the droplet shape and only the viscous dissipation (by the liquid motion inside the droplet) was considered as the energy dissipation. However, in practice, the charge density varies along the surface (because of the surface-shape irregularity) and the force required to move the contact line between the three phases (i.e., between the droplet, substrate and the surrounding gas) may be another source of the energy loss during the spreading process.

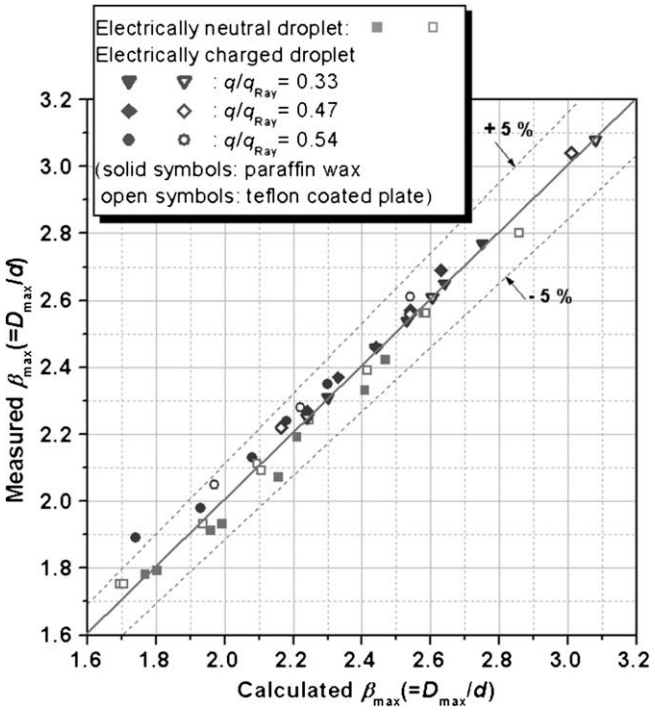

Fig. 9. Assessment of the improved model for the maximum spreading ratios.

The present model is applicable only to the case of droplet collision against dielectric substrates because the amount of the electric charge was conserved (i.e., there is no electric discharge through the substrate) during the spreading process. However, various kinds of substrates are being used in engineering applications and their electrical characteristics should be considered in predicting the spreading behavior of charged droplets, which is left as a future work.

4. Conclusion

The spreading phenomena of electrically charged droplets impacting on dielectric substrates were studied both experimentally and analytically, and the results are summarized as follows:

- The maximum spreading ratios of electrically charged droplets are higher than those of the neutral droplets when the impacting conditions (velocity and size of the droplet) remain the same; moreover, the difference becomes larger as the electric charge ratio increases.
- An improved model was proposed to predict the maximum spreading ratio of the electrically charged droplets. This model is based on modification of the liquid–gas and the liquid–solid interfacial tensions, expressed as a function of the electric charge ratio and the surface area ratio. The improved model predicts the maximum spreading ratio within an accuracy of ± 5%.

Acknowledgements

This work was performed under the auspices of Samsung Heavy Industries Co., Ltd. (Project Title: Development of Electrostatic Spraying Equipment and Process for Ship Painting), Combustion Engineering Research Center (CERC) and the BK-21 program.

References

Bailey, A.G., 1988. Electrostatic Spraying of Liquids. Wiley, New York.
Bateni, A., Laughton, S., Tavana, H., Susnar, S.S., Amirfazli, A., Neumann, A.W., 2005. Effect of electric fields on contact angle and surface tension of drops. J. Colloid Interf. Sci. 283, 215–222.
Bateni, A., Amirfazli, A., Neumann, A.W., 2006. Effects of an electric field on the surface tension of conducting drops. Colloids Surfaces A 289, 25–38.
Carey, V.P., 1992. Liquid–Vapor Phase Change Phenomena. Hemisphere, Washington, DC.
Chandra, S., Avedisian, C.T., 1991. On the collision of a droplet with a solid surface. Proc. R. Soc. Lond. A 432, 13–41.
Digilov, R., 2000. Charge-induced modification of contact angle: the secondary electrocapillary effect. Langmuir 16, 6719–6723.
Fowkes, F.M., 1963. Additivity of intermolecular forces at interfaces: 1. Determination of the contribution to surface and interfacial tensions of dispersed forces in various liquids. J. Phys. Chem. 67, 2538–2541.
Girifalco, L.A., Good, R.J., 1957. A theory for the estimation of surface and interfacial energies: 1. Derivation and application to interfacial tension. J. Phys. Chem. 61, 904–909.
Girifalco, L.A., Good, R.J., 1958. A theory for the estimation of surface and interfacial energies: 2. Application to surface thermodynamics of teflon and graphite. J. Phys. Chem. 62, 1418–1421.

Girifalco, L.A., Good, R.J., 1960. A theory for the estimation of surface and interfacial energies: 3. Estimation of surface energies of solids from contact angle data. J. Phys. Chem. 64, 561–565.

Kang, K.H., Kang, I.S., Lee, C.M., 2003. Wetting tension due to Coulombic interaction in charge-related wetting phenomena. Langmuir 19, 5407–5412.

Kline, S.J., 1985. The purposes of uncertainty analysis. J. Fluids Eng. 107, 153–160.

Lee, J., Moon, H., Fowler, J., Schoellhammer, T., Kim, C.J., 2002. Electrowetting and electrowetting-on-dielectric for microscale liquid handling. Sensors Actuators A 95, 259–268.

Li, D., Neumann, A.W., 1990. A reformulation of the equation of state for interfacial tensions. J. Colloid Interf. Sci. 137, 304–307.

Li, D., Neumann, A.W., 1992. Contact angles on hydrophobic solid surfaces and their interpretation. J. Colloid Interf. Sci. 148, 190–200.

Mao, T., Kuhn, D.C.S., Tran, H., 1997. Spread and rebound of liquid droplets upon impact on flat surfaces. AIChE J. 43, 2169–2179.

Park, H., Carr, W.W., Zhu, J., Morris, J.F., 2003. Single drop impaction on a solid surface. AIChE J. 49, 2461–2471.

Pasandideh-Fard, M., Qiao, Y.M., Chandra, S., Mostaghimi, J., 1996. Capillary effects during droplet impact on a solid surface. Phys. Fluids 8, 650–659.

Rayleigh, J.W.S., 1945. The Theory of Sound. Dover, New York.

Ryu, S.U., Lee, S.Y., in press. Revisit of spread-rebound transition criterion in droplet-wall impingement. Int. J. Transport Phenomena.

Vallet, M., Berge, B., Vovelle, L., 1996. Electrowetting of water and aqueous solutions on poly(ethylene terephthalate) insulating films. Polymer 37, 2465–2470.